journal

J. Am. Ceram. Soc., 93 [6] 1639–1649 (2010)
DOI: 10.1111/j.1551-2916.2010.03662.x


# Sintering, Phase Stability, and Properties of Calcium Phosphate-Mullite Composites

Shekhar Nath,[‡] Krishanu Biswas,[‡] Kaishi Wang,[§] Rajendra K. Bordia,[§] and Bikramjit Basu[†,‡]

[‡]Department of Materials and Metallurgical Engineering, Indian Institute of Technology Kanpur, Kanpur-208016, UP, India

[§]Department of Materials Science & Engineering, University of Washington, Seattle, Washington 98195-2120

**In this contribution, we report the results of a study to probe into the combined effect of the sintering conditions and mullite ($3Al_2O_3 \cdot 2SiO_2$) addition (upto 30 wt%), on the densification mechanism, phase assemblage, and microstructure development in calcium phosphate (CaP)-mullite composites. The experimental results reveal that close to 95% theoretical density can be achieved by sintering the compositions in the temperature range of 1300°–1350°C. Finer scale microstructural analysis using transmission electron microscopy reveals the presence of both β- and α-TCP ($Ca_3(PO_4)_2$–tricalcium phosphate) and a crystalline residue of gehlenite at triple junctions. The shrinkage kinetics of the composites have been analyzed to qualitatively understand the sintering mechanisms. For the composites, solid-state sintering in the initial stage, followed by liquid-phase sintering at or near the sintering temperature are postulated to explain the effect of temperature and volume fraction of the second phase. Some important features of the liquid-phase sintering have been discussed using the $CaO$–$Al_2O_3$–$SiO_2$ ternary phase diagram. A comparison with the earlier published results reveals that a better combination of long-crack fracture toughness, compressive strength, and flexural strength can be obtained with the newly developed composites.**

## I. Introduction

HYDROXYAPATITE [$Ca_{10}(PO_4)_6(OH)_2$, HAp], the most important CaP material, is widely recognized as a highly biocompatible and bioactive material; however, its poor mechanical properties limit its use as an implant material.[1] Therefore, the motivation for developing HAp-based composites stems from the requirement to fabricate materials with improved strength and toughness without compromising its biocompatibility.[2] To this end, HAp could be used in combination with another metal/ceramic phase, which can improve the physical properties of HAp without deteriorating its biocompatibility. To date, the widely studied HAp-based biocomposites include HAp-alumina composites,[3,4] HAp-zirconia,[5,6] HAp-bioglass[7], and HAp-$HAp_w$ (whisker)[8] composites, etc. In all the above-mentioned HAP-based systems, the optimization of sintering parameters as well as phase stability have been a major issue.

A common phenomenon reported for the sintering of HAp-based composites is the dissociation of HAp due to dehydroxylation (removal of $OH^-$ ion) resulting in biphasic calcium phosphate (BCP—mixture of HAp and tricalcium phosphate (TCP)). In recent years, the microstructure containing BCP phases has received attention as an ideal bone substitute due to its controlled degradability.[9] The literature reports indicate that it is possible to alter HAp:TCP ratio to form BCP of desired properties.[10] In one of the earlier studies, it was observed that 10 wt% phosphate glass addition to HAp-composites led to a partial dissociation of HAp to TCP.[11]

With an aim to develop lightweight biocompatible material, the choice of mullite as a ceramic reinforcement has been made in the present work, because of the fact that mullite has a lower density (3.06 g/cm$^3$) and a higher hardness (12–15 GPa) than HAp and a moderate fracture toughness ($\sim 3$ MPa $\cdot$ m$^{0.5}$). Mullite, an important structural ceramic material, is a compound with larger solubility of silica in alumina and has been investigated for a long time as a refractory material. While developing HAp-mullite composites, the hypothesis was that mullite will not react directly with HAp or TCP. In our recent investigation, it has been shown that mullite reacts only with CaO, one of the dissociation products of HAp.[12] Therefore, in HAp-mullite composites, maximum retention of CaP is possible, which is unlikely for other HAp-based composites. For example, in case of HAp-alumina and HAp-zirconia composites, the second phases (alumina[3,4] or zirconia[5,6]) can directly react with CaP phases (HAp or TCP). Another benefit of using mullite particle is that good densification can be achieved due to liquid-phase sintering,[12] which is absent in other HAp-based composites.

With this background, the present paper describes the densification kinetics of HAp-mullite composite mixtures and various sintering events during heat treatment. It also describes the phase assemblages in sintered bodies as a function of mullite addition as well as sintering temperatures. Detailed thermal analysis (dilatometer) of the composites has been conducted and correlated with the X-ray diffraction (XRD), scanning electron microscope (SEM), Fourier transform infrared spectroscopy (FTIR), and transmission electron microscopy (TEM) results to develop a qualitative understanding of the sintering mechanisms. Also, the mechanical properties of the developed composites are briefly summarized to illustrate the advantage of using mullite as a reinforcement.

## II. Experimental Procedure

### (1) Starting Powders and Composite Synthesis

HAp was synthesized by the widely reported solution–precipitation route.[13] The precursor materials were calcium oxide (CaO, Merck, Darmstadt, Germany) and phosphoric acid ($H_3PO_4$). XRD of as-synthesized HAp, calcined at 800°C reveals the X-ray peaks corresponding to the pure HAp phase. A Ca/P atomic ratio of 1.64 was obtained by inductive-coupled plasma-atomic emission spectroscopy (ICP-AES: spectroflame modula FTM08, Spectro GMBH, Kleve, Germany) from the HAp powder calcined at 800°C. Therefore, in the present set of experiments,

H.-E. Kim—contributing editor

Manuscript No. 26143. Received April 13, 2009; approved January 12, 2010.
This work was financially supported by Department of Biotechnology, Government of India.
[†]Author to whom correspondence should be addressed. e-mail: bikram@iitk.ac.in

the synthesized HAp powder was quite pure and stoichiometric (the Ca/P of stoichiometric HAp is 1.67). Commercially available phase-pure mullite ($D_{50} \sim 1.04$ μm, KCM Corporation, Nagoya, Japan) was used as a reinforcement.

In the production of the composites, varying amount of mullite (10–30 wt%) was ball milled with HAp for 16 h in acetone using agate balls as the milling media to break the agglomerates. Various ceramic compositions are designated as HAp$x$M (where M≡mullite, $x = 10$, 20, 30 wt% of mullite) throughout the text. The ball-milled powders were subsequently compacted in a hydraulic uniaxial cold press at a pressure of around 92 MPa to obtain green bodies of a cylindrical shape of 12 mm diameter. The powder compacts were subsequently sintered at various temperatures upto 1400°C in air (Nabertherm supercanthal, Lilienthal, Germany). In all sintering experiments, the heating rate was 5°C/min. After the sintering processes, a typical sintered disk had a thickness of 1–2 mm. This specific size and shaped samples were used to study the sintering, microstructure, and phase assemblages. In order to analyze the shrinkage behavior of various compositions, dilatometry experiments (Netzsch 402 C Dilatometer, Netzsch Instruments Inc, Burlington, MA) were carried out at constant heating rates (5°C/min) in air.

### (2) Characterization of Sintered Composites

The density of each sintered sample was measured three to four times by the Archimedes's principle using water as the fluid. XRD analysis was carried out using Cu$K\alpha$ radiation ($\lambda = 1.5418$ Å) to identify different phases in the starting powders as well as sintered materials. FTIR (FT-IR, vortex 70, Bruker, Ettlingen, Germany) was conducted on powders of sintered samples to identify the different chemical bonds in the composites.

Before to SEM observations, the sintered disks were polished using diamond paste to 1 μm surface finish and then ultrasonically cleaned. All the polished samples were thermally etched at a temperature of 100°C lower than the sintering temperature. The compositional variations in different areas of the microstructure were studied using energy-dispersive X-ray spectroscopy (EDS, attached to SEM (Philips, FEI-Quanta operated at 20 kV, Eindhoven, the Netherlands)). The TEM analysis of all composite composition samples (HAp10M, HAp20M, and HAp30M, all sintered at 1350°C for 2 h) was performed using a TEM (JEOL 2000 FXII and Technai F, Tokyo, Japan) operated at 200 kV. Electron transparent thin foils were prepared by the standard sample preparation technique, which included grinding, dimpling, and subsequent ion milling using argon gas ions at 5 kV under an angle of 4°–5° tilt.

For each material composition, the sample with the highest density was characterized for basic mechanical properties. The long-crack fracture toughness, flexural strength, and compressive strength were measured for at least three replicate samples. The fracture toughness was measured using a single edge V-notched beam (SEVNB) technique. For SEVNB testing, a V-shaped notch was introduced along the height of the specimen (dimensions: 20 mm × 4 mm × 4 mm, cut from ~25 mm diameter sintered disk) using a diamond saw and a razor blade with diamond abrasive paste on a commercial V notch preparation machine (Scientific Testing Devices, Frankfurt, Germany). The notch radius for all the samples were <10 μm and varied in the range of 5–9 μm. The notched samples were then fractured using a four-point bending set up on a universal testing machine (Instron, TTMCL, Chennai, India). The fracture load was obtained and fracture toughness was calculated using the established equations, as reported by Choi and colleagues.[14,15]

The flexural strength of the composite was measured using a three-point bending test. For this purpose, sintered disks of ~25 mm diameter with 4–5 mm thickness were prepared. A sample dimension of 20 mm × 4 mm × 4 mm were cut from the disk. For the evaluation of compressive strength, the sintered samples of 4 mm diameter and 4–5 mm height were used. In both the cases, the samples were tested with a constant crosshead speed of 0.05 mm/s. During the entire tests, the load–displacement was recorded using a computer attached to a universal testing machine (Instron, TTMCL).

## III. Results

### (1) Densification

The sintered density for HAp monolith as well as the composites, at various temperatures is shown in Fig. 1. Each data point in Fig. 1 represents an average value of five or more sintering experiments on the same starting powder composition. For pure HAp, the density increases with temperature to a maximum of ~99%$\rho_{th}$ at 1200°C. In case of HAp10M, the sintered density systematically increases in the temperature window of 1000°–1300°C. The densification changes sharply in the temperature range of 1300°–1350°C, followed by a negligible change in density as the sintering temperature is increased to 1400°C. In contrast, a different behavior is observed for HAp20M and HAp30M samples. For these two composites, the density sharply increases in the temperature window of 1200°–1350°C, and then decreases when the sintering temperature is increased further. It is also clear that the density of HAp20M composite is higher than those of 10 and 30 wt% composites in the temperature window of 1200°–1300°C. Note that in all cases, the theoretical density has been calculated using the composition of the starting powder mix and the rule of mixtures. Considering the sintered phases and the phases in the starting powder, the differences in theoretical density of starting phase and dissociated phases are very small. For example, the density of HAp, TCP, mullite, gehlenite, and CaO is 3.15, 3.06, 3.05, 3.02, and 3.35 gm/cm$^3$, respectively. Only, one of the minute dissociated phases, alumina has a density much higher than other phases (3.9 gm/cm$^3$). Therefore, the volume changes as well as the density changes would be mostly from densification or pore elimination. From this point of view, the theoretical density calculated based on initial composite compositions would be the representative theoretical density of sintered products.

In order to investigate the linear shrinkage during sintering, dilatometric studies were conducted and the shrinkage data are plotted in Fig. 2. In Fig. 2(a), the % linear shrinkage ($\Delta L \times 100/L_0$, $\Delta L$ = length change at any given temperature ($T$) with respect to initial length $L_0$) versus temperature (upto 1400°C) for pure HAp and mullite as well as for composites are plotted as a function of temperature for a constant heating rate of 5°C/min. The corresponding shrinkage rate is plotted in Fig. 2(b) as a

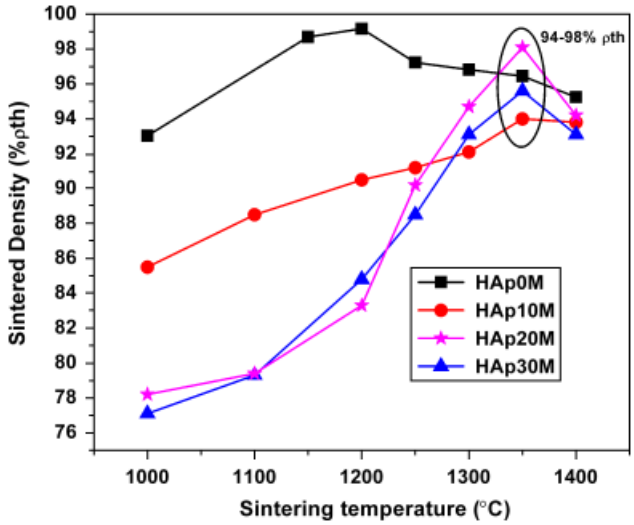


**Fig. 1.** Final sintered density as a function of sintering temperature for hydroxyapatite (HAp) mullite composites. Results are reported for composites with varying amounts of mullite (up to 30 wt%) For comparison, the results for pure HAp are also reported. The theoretical density ($\rho_{th}$) is calculated based on the starting composition of the composites. All samples were held at the sintering temperature for 2 h.

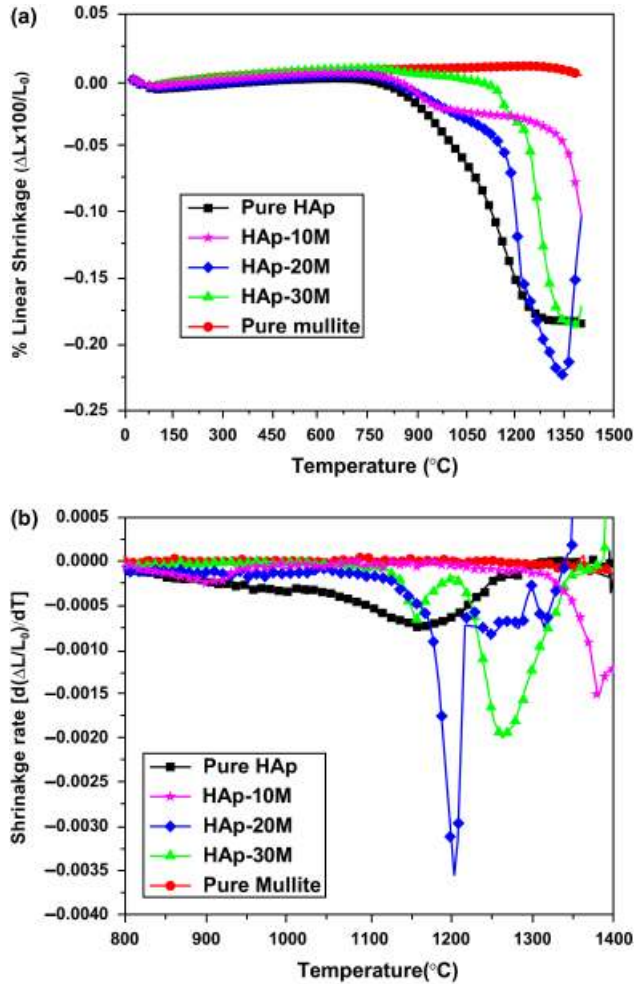


**Fig. 2.** (a) Shrinkage as a function of temperature of hydroxyapatite (HAp), mullite, and HAp mullite composites up to 1350°C. The plot shows linear dimension change (strain) during constant rate heat treatment (5°C/m). (b) The linear shrinkage strain rate as a function of temperature during constant rate heat treatment (5°C/m) up to 1350°C for HAp, mullite, and HAp mullite composites.

function of temperature. The shrinkage rate in Fig. 2(b) is determined by differentiating the curves of Fig. 2(a). These results show that pure HAp starts to densify at around 800°C and continues densifying up to 1200°C. At this temperature, the densification is complete. Further heating up to 1400°C does not lead to any noticeable shrinkage. Also, the recorded shrinkage curve clearly indicates a solid-phase sintering (broad peak in densification rate, Fig. 2(b)). For pure mullite, no measurable shrinkage can be observed in the temperature region of RT to 1330°C. At $T > 1330$°C, a noticeable shrinkage indicating early-stage solid-state sintering is observed.

The HAp-mullite composites exhibit a very different densification behavior. Broadly speaking, the densification behavior of all the composites can be considered as a two-stage phenomenon. The first stage is characterized by an early onset and a low densification rate. The second stage is characterized by a sharp increase in densification rate at higher temperatures. The two stages are very clearly observed for the HAp20M and HAp30M samples. As the mullite percentage increases, the onset of the solid-state sintering is delayed and the associated shrinkage is also reduced.

### *(2) Phase Evolution*

Figure 3 plots the XRD patterns of pure HAp, HAp-10, -20, and -30 wt% mullite, sintered under different conditions. XRD results in Fig. 3(I) indicate that as synthesized HAp is stable during sintering upto 1200°C (Figs. 3(I)(a) and (b)) and the presence of β-TCP can be observed after sintering at and above 1300°C (Figs. 3(I)(c) and (d)). In contrast, the stability of HAp shows a different trend in the presence of mullite. For example, in case of HAp10M composition (Fig. 3(II)(a)), it can be noted that HAp partially dissociates to β-TCP, when sintered at 1200°C. When the sintering temperature is increased to 1300°C, α-TCP starts to form (Fig. 3(II)(c)). The XRD spectra presented in Figs. 3(II)(d) and (II)(e) compare the phase evolution in HAp10M composition sintered at 1350°C for 2 and 6 h, respectively. It is clear that the longer soaking time does not lead to any changes in phase assemblages, and therefore the various phase combination in sintered HAp10M are quite stable against further dissociation and additional reactions. The presence of HAp could be observed up to 1350°C (Fig. 3(II)(e)). However, at and above 1400°C, HAp is almost completely dissociated to α-TCP phase (Fig. 3(II)(f)). The dissociation product of HAp, i.e. CaO is also detectable in the XRD spectra for all the samples. Another interesting point is that the sintering of HAp10M at $T > 1200$°C leads to BCP (a mixture of HAp and TCP) matrix in the sintered composite.

The dissociation of HAp and the resulting phase evolution, however, is very different for HAp20M and HAp30M samples, as shown in Figs. 3(III) and (IV). For example, the primary HAp phase is almost completely dissociated to β-TCP after sintering at 1200°C, in case of HAp20M sample (Fig. 3(III)(b)). Such a dissociation also produces CaO. Beyond 1350°C, the transformation of β- to α-TCP was also noted (Figs. 3(III)(e) and (f)). The peaks of mullite are also observed at all sintering temperatures. Two additional phases are also detected in XRD and these are gehlenite and alumina. A similar phase evolution was observed in HAp30M samples (Fig. 3(IV)). However, in this case, the formation of α-TCP was only observed at and above 1400°C; otherwise, β-TCP is the dominant phase at all sintering temperatures. In Fig. 3(IV)(c)–(e), XRD results from samples sintered for different times at 1300°C (2, 4, and 6 h) are shown. All these spectra are similar, indicating that the phase changes occur quite rapidly at these temperatures.

In Fig. 4, the peak ratio of the most intense peaks of HAp, TCP, and mullite, extracted from XRD plots, is plotted for the composites (from Figs. 3(II–IV)). Although, such a peak ratio does not exactly reveal the quantitative ratio, it can provide approximate semiquantitative information about the phase content. Fig. 4(a) clearly demonstrates the difference in behavior of HAp10M with HAp20 and HAp30M. The dissociation of HAp to TCP clearly occurs at much lower temperatures for the 20 and 30 wt% composites. Figure 4(b) represents the ratio of the most intense peak of the mullite and total calcium phosphate (CaP = HAp and TCP) as a function of temperature. It is quite clear from Fig. 4(b) that the amount of mullite decreases with an increasing sintering temperature, irrespective of composite compositions.

### *(3) FTIR Analysis*

To obtain complimentary information on the decomposition of HAp, FT-IR analysis has been conducted. Figures 5(a) and (b) show the FT-IR results for HAp10M and HAp30M, sintered at varying temperatures. In both the figures, the spectra show the characteristic band due to $PO_4^{3-}$ groups at (see the Fig. 5(a)) 938, 420, 1125, and 567 $cm^{-1}$ for $\nu_1$, $\nu_2$, $\nu_3$, and $\nu_4$ vibrations respectively.[16] A very weak O–H stretching vibration band[17] is observed at 3570 $cm^{-1}$ and a libration vibration band at 612 $cm^{-1}$ in the HA-10 wt% mullite sample (Fig. 5(a)). This observation supports the weak peaks of retained HAp, also detected using XRD (Fig. 3(II)). At higher mullite content or at higher sintering temperature (1300°C), the characteristic O–H band is absent, implicating the dehydroxylation as a result of HA decomposition.[18] Therefore, the peaks corresponding to $PO_4^{3-}$ in these samples indicate the presence of the TCP phase, which supports the XRD observations shown in Figs. 3(II–IV). A broad peak at around 3450 $cm^{-1}$, corresponding to the absorbed moisture during sample preparation is evident from the FTIR plots in Figs. 5(a) and

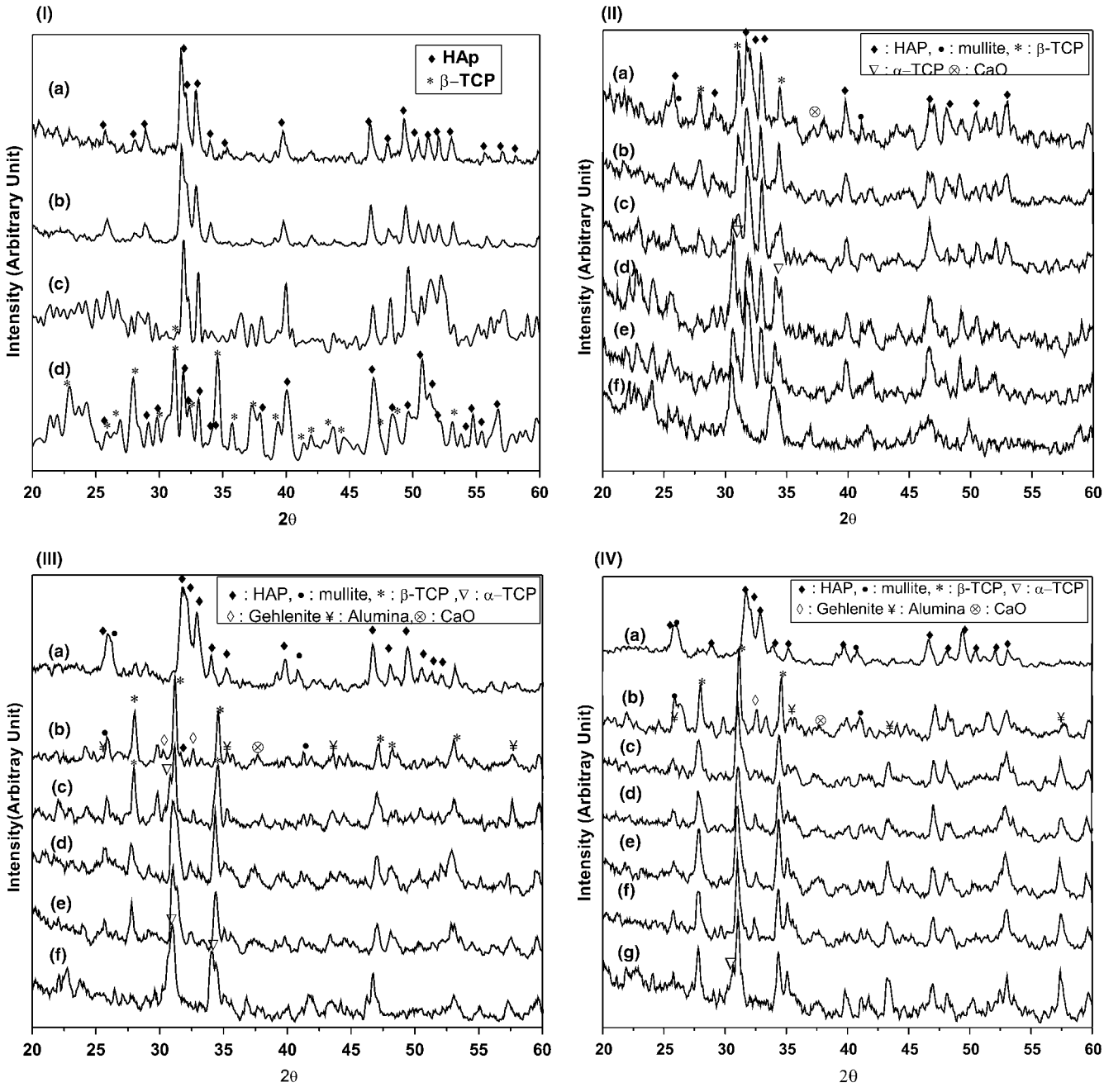


**Fig. 3.** Powder X-ray diffraction spectra from (I) pure hydroxyapatite (HAp), sintered at various temperatures: (a) 1000°C, (b) 1200°C, (c) 1300°C, and (d) 1400°C for 2 h. Only the major three peaks are indicated in the plots, (II) HAp10 wt% mullite composites, sintered under various conditions: (a) 1200°C for 2 h, (b) 1250°C for 2 h, (c) 1300°C for 2 h, (d) 1350°C for 2 h, (e) 1350°C for 6 h, and (f) 1400°C for 2 h, (III) HAp 20 wt% mullite: (a) ball-milled powder after 16 h milling, (b) 1200°C for 2 h, (c) 1250°C for 2 h, (d) 1300°C for 2 h, (e) 1350°C for 2 h, and (f) 1400°C for 2 h, (IV) HAp 30 wt% mullite. (a) After ball milling for 16 h (b) 1200°C for 2 h, (c) 1300°C for 2 h, (d) 1300°C for 4 h, (e) 1300°C for 6 h, (f) 1350°C for 2 h, and (g) 1400°C for 2 h.

(b). In addition to the above-mentioned peaks, few other peaks are also detected at around 2000, 2350, and 2930 $cm^{-1}$. These peaks are not the characteristics of the samples, as FT-IR analysis of the KBr pellet (free run) reveals that these peaks appear due to moisture and $CO_2$ absorption during FT-IR sample preparation.

### *(4) Microstructure Analysis*

The microstructure of pure HAp, sintered at 1200°C for 2 h reveals a dense, pore-free microstructure (Fig. 6(a)). From Fig. 6(a), the microstructure can be characterized as bimodal with the presence of coarse grains dispersed in the fine grain matrix. However, for the HAp-mullite composite microstructure, pores are present (Fig. 2(b)) with varying size and distribution, depending on the sintering conditions. Typical pores, often irregular shapes, with a size in the range of 2–5 μm are observed. The origin of pores can be explained either by the difficulty in sintering in the presence of mullite or due to gas evolution as a result of the dissociation reaction. As will be discussed later, the dissociation of HAp during sintering releases $H_2O$ gas. In Fig. 6(b), the SEM image of the polished surface of HAp20M sample, sintered at 1350°C for 2 h is shown. EDS analysis reveals the dominant phase as HAp/TCP, and the grain-boundary phase is an (Al–Si)-rich phase. Figure 6(c) is a higher magnification image of this composite sintered at 1350°C for 2 h. The coarser HAp (or TCP) grains are surrounded by small calcium-alumino-silicate grains. Gold peaks are due to the gold coating used for SEM analysis.

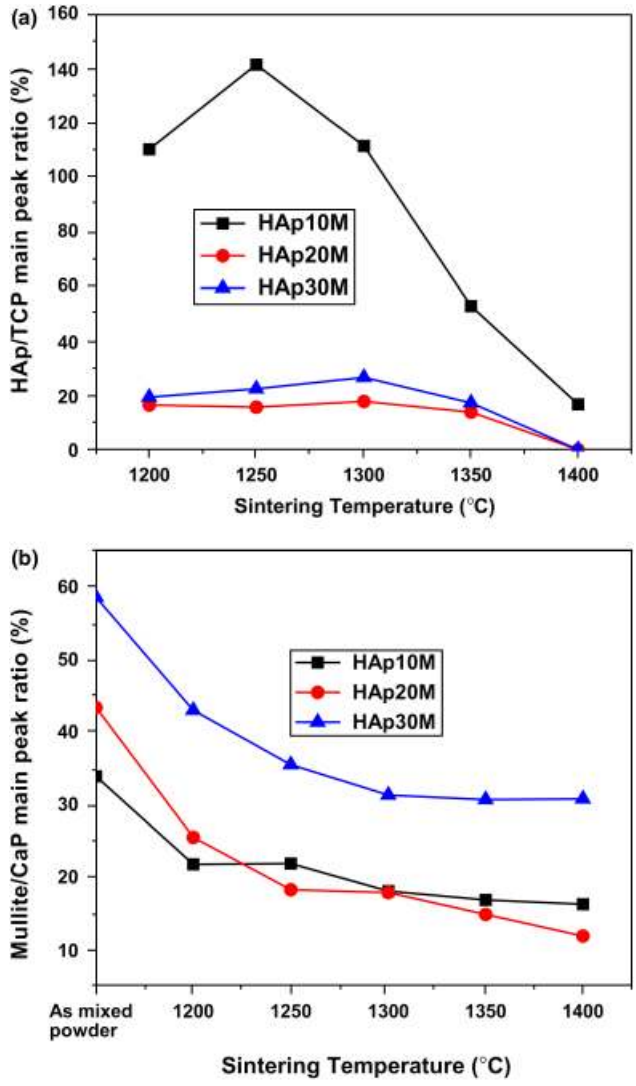


**Fig. 4.** (a) hydroxyapatite (HAp) and tricalcium phosphate (TCP) ($\alpha+\beta$) main peak intensity ratio with a variation of sintering temperature for HAp (10-30) mullite composite samples. (b) Mullite to calcium phosphate main peak intensity ratio as a function on sintering temperature for HAp (10–30) mullite composite samples.

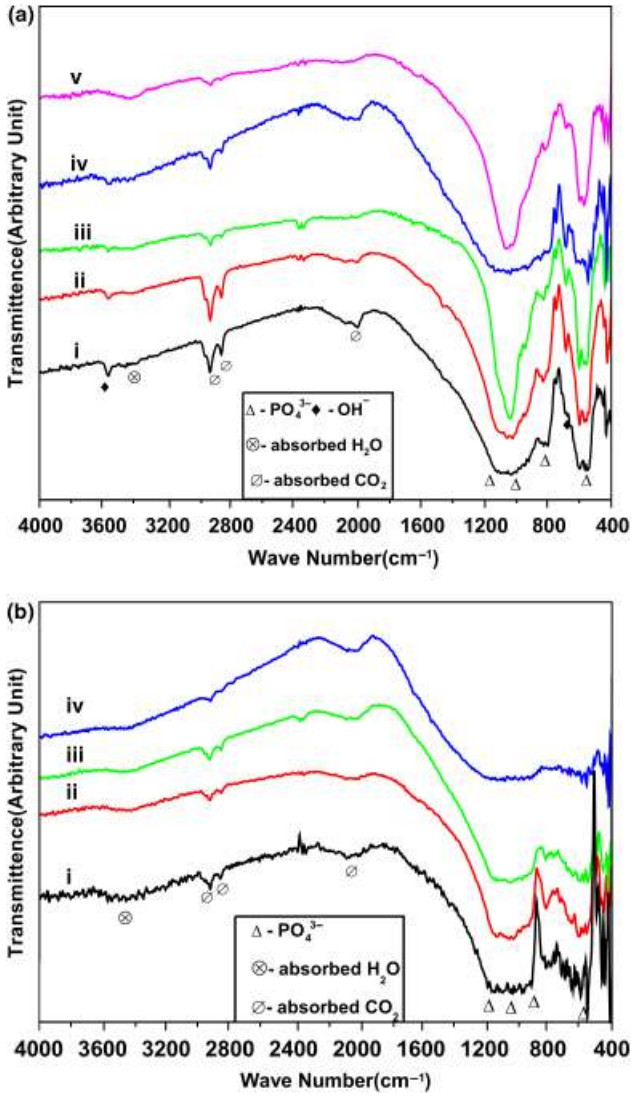


**Fig. 5.** Fourier transform infrared spectroscopic spectra after sintering at different temperatures for (a) hydroxyapatite (HAp)10M samples sintered at (i) 1200°C for 2 h, (ii) 1250°C for 2 h, (iii) 1300°C for 2 h, (iv) 1350°C 2 h, and (v) 1400°C for 2 h in air atmosphere. (b) HAp30M samples sintered at (i) 1300°C for 2 h, (ii) 1300°C for 4 h, (iii) 1350°C for 2 h, (iv) 1400°C 2 h and in air atmosphere.

A detailed TEM study has been conducted for all the composites to decipher the phases, their morphologies as well as reaction products. The results of TEM analysis of HAp20M (sintered at 1350°C for 2 h) are presented in Fig. 7, which is a low-magnification bright-field image showing morphologies of the different phases. The microstructure reveals large grains of transformed TCP and needle-shaped mullite along with the presence of dissociation/reaction products. The selected area diffraction (SAD) patterns from different phases observed in the microstructure are also presented and indexed in Fig. 7. From the SAD patterns (Figs. 7(b)–(e)), the presence of TCP, mullite, and the reaction product gehlenite as well as the dissociation product CaO, can be confirmed. The presence of undissociated HAp grains could also be detected (Fig. 7(f)) in the TEM study, although the number of HAp grains is fewer than TCP grains. The interesting observation to be noted here is that for HAp20M composites, sintered at 1350°C for 2 h, although the XRD pattern (Fig. 3(III)(e)) does not show any peaks from the HAp phase, the presence of HAp is evident from the SAD pattern (Fig. 7(f)). The mullite phase can be easily identified by the typical needle-like shape. The size of the randomly oriented mullite needles are $\sim$2 μm. From TEM analysis, it appears that gehlenite nucleates from the liquid phase during sintering. Similar observations have been made in case HAp10M and HAp30M composites.[12] The microstructural analysis of samples containing 10, 20, and 30 wt% mullite reveals that the reaction product during sintering at an elevated temperature is liquid. Because gehlenite nucleates from this liquid phase due to the reaction between mullite and CaO (a dissociation product of HAp), it develops an interface with TCP (dissociation product of HAp), mullite, and CaO. From Fig. 7, it appears that the interface between the mullite needles and ghelenite is sharp. On the other hand, the interface between ghelenite/TCP or ghelenite/CaO are diffuse, which is a clear signature that gehlenite nucleates at TCP/mullite/CaO triple junctions and grows into TCP and CaO grains.

It is to be noted here that the initial precursor mullite particles were not needle shaped. However, a needle-like morphology of mullite is observed in sintered ceramics. It has been reported that mullite grows in equiaxed morphology in the presence of microstructural constraints.[19] This happens in case of solid-state sintering of pure mullite[20] and mullite-based composites.[21] However, in an unconstrained microstructure (e.g., during liquid-phase sintering) due to the anisotropic nature of the growth of rhombohedral mullite, they can grow anistropically[20,22,23]

resulting in elongated mullite grains. In this investigation, it is believed that the formation of calcia–alumina-silica liquid phase helps the mullite phase to grow in an unconstrained matrix leading to the observed morphology. Similar microstructures were obtained for HAp10M and HAp30M samples.

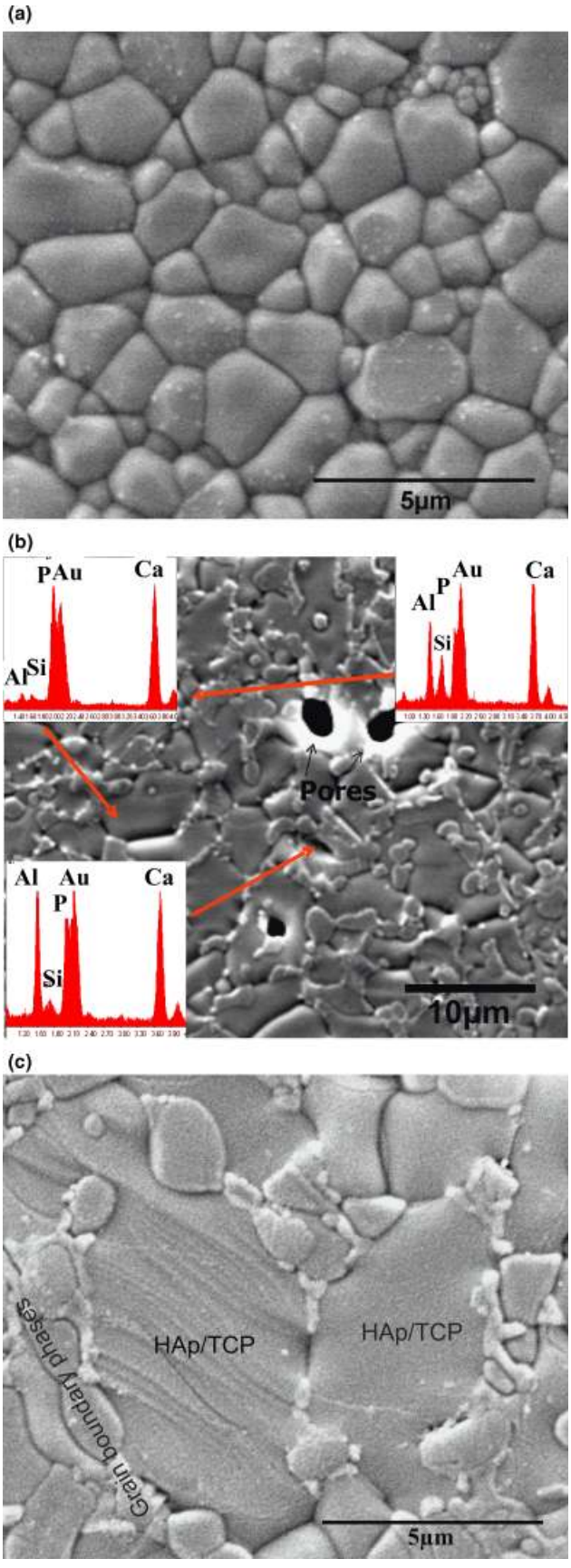


**Fig. 6.** (a) Microstructure of pure hydroxyapatite (HAp) sintered at 1200°C for 2 h. (b) Representative microstructure from polished and thermally etched surface of HAp-20 wt% mullite samples (sintered at 1350°C for 2 h) shows HAp/tricalcium phosphate (TCP) matrix with calcium-alumino-silicate as grain-boundary (GB) phase. energy-dispersive X-ray spectroscopic analysis shows the composition of the matrix phase as well as the GB phase. Presences of intragranular pores are predominantly observed for this sample. Similar microstructure obtained for HAp 10 wt% mullite and HAp 30 wt% mullite. (c) The high-magnification image shows bigger grains of HAp-TCP matrix phase and smaller grains of calcium-alumino-silicate grains GB phase.

### *(5) Mechanical Properties*

Table I presents fracture toughness, flexural strength, and compressive strength obtained for pure HAp, HAp10M, HAp20M, and HAp30M composites. The fracture toughness value of pure HAp is $\sim 0.6\ MPa \cdot m^{0.5}$. For the HAp-mullite composite, significant improvement in fracture toughness is observed. For HAp20M and HAp30M composites a fracture toughness of $\sim 1.5\ MPa \cdot m^{0.5}$ was obtained, which is almost 2.5 times higher than pure HAp. The flexural strength values show that HAp20M has the highest flexural strength among the composites, which is $\sim 80$ MPa. HAp30M composites also have a flexural strength of 75 MPa, close to that of HAp20M. Both the samples were sintered at 1350°C for 2 h. For HAp10M sample, the maximum flexural strength (51 MPa) was from the sample sintered at 1400°for 2 h. The compressive strength values of HAp-mullite composites also exhibit a superior improvement with an increasing mullite content. For pure HAp, the compressive strength was recorded as 54 MPa, whereas for HAp10M, HAp20M, and HAp30M samples, the average strength values were measured as 127, 233, and 381 MPa, respectively.

## IV. Discussion

In this section, the experimental results obtained from dilatometry, XRD, FT-IR, SEM, and TEM will be correlated and following this, an attempt will be made to understand the sintering behavior with the help of $CaO–Al_2O_3–SiO_2$ ternary phase diagram.[24] A brief discussion on mechanical properties as well as a comparison with the literature results will also be made.

### *(1) HAp Stability*

The stability of HAp as a function of sintering temperature and mullite content will be discussed on the basis of XRD and microstructural investigation. It is evident from the Figs. 4(a) and (b) that a higher amount of mullite is consumed as the sintering temperature increases. For the HAp20M (Fig. 3(III)) and HAp30M (Fig. 3(IV)), the dissociation of HAp occurs much faster than HAp10M due the interaction of HAp with mullite. At 1350°, β-TCP transforms to α-TCP. XRD results also reveal that the presence of higher amount of mullite retards the conversion of β-TCP to α-TCP. In case of 10 and 20 wt% mullite composites, the presence of a considerable amount of α-TCP is noticeable, but in case of 30 wt% mullite, no α-TCP is present upto 1350°C.

One possible hypothesis for these observations is that in addition to the temperature, the mullite promotes the decomposition of HAp to CaO and TCP. Thereafter, the mullite reacts with the CaO to form calcium-alumino-silicate phase (gehlenite) and the favorable nature of this reaction accelerates the decomposition of HAp. For the particle sizes used in this work, it may be possible that the optimal numbers of mullite/HAp contacts are present for the 20 wt% composite, and thus this composite undergoes the most extensive sintering reactions. Further addition of mullite leads to more of mullite/mullite contacts, which do not participate in the reaction, and in contrast act as non-densifying inclusions in a sinterable matrix.[25–27]

The density of pure HAp (99.17%$\rho_{th}$) peaks at 1200°(Fig. 1), which is followed by a gradual decrease with an increasing sinte-

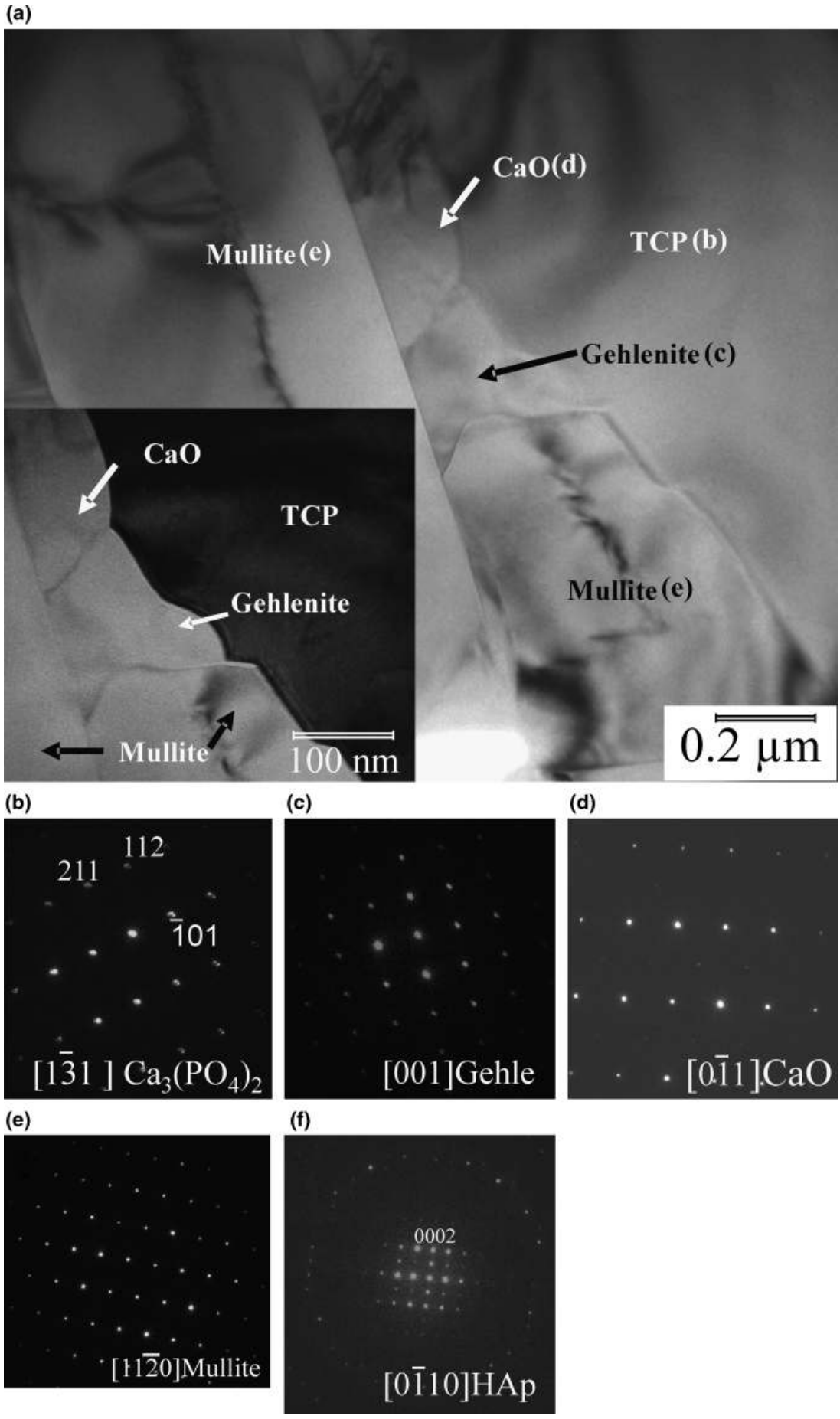


**Fig. 7.** (a) Low-magnification bright-field image showing the interfacial reaction products during sintering. (b)–(f) Selected area diffraction (SAD) patterns obtained from various phases. The inset in (a) shows a higher magnification image of the region near the hydroxyapatite (HAp)-mullite region with HAp grain oriented along direction. Some of the grains remain untransformed. SAD from one such HAp grain is shown in (f).

**Table I. Mechanical Properties (An Average of at Least Five Samples) of Pure Hydroxyapatite (HAp) and Various HAp-Mullite Composites Sintered Under optimized Conditions**

| Starting powder composition | Sample designation | Sintering conditions | SEVNB toughness ($K_{IC}$, MPa · $m^{0.5}$) | Flexural strength (MPa) | Compressive strength (MPa) |
|---|---|---|---|---|---|
| HAp-0 wt% mullite | Pure HAp | 1200°C for 2 h | 0.6 ± 0.01 | — | 54.2 ± 0.01 |
| HAp-10 wt% mullite | HAp10M | 1400°C for 2 h | 0.9 ± 0.05 | 51 ± 1.2 | 126.8 ± 25.9 |
| HAp-20 wt% mullite | HAp20M | 1350°C for 2 h | 1.5 ± 0.17 | 80 ± 3.5 | 232.7 ± 33.5 |
| HAp-30 wt% mullite | HAp30M | 1350°C for 2 h | 1.5 ± 0.13 | 75 ± 2.7 | 380.9 ± 14.5 |

SEVNB, single edge V-notched beam.

ring temperature. This observation corroborates the XRD observation that at and above 1200°C, HAp dissociates to β-TCP, which has a slightly lower density (3.06 g/cm$^3$) than HAp (3.16 g/cm$^3$). With the increase in sintering temperature, β-TCP further transforms into α-TCP, which has a lower density (2.81 g/cm$^3$). Our experimental results are in line with the earlier results reported in the literature. Yin *et al.*[28] have shown theoretically as well as experimentally that β-TCP is much more stable than α-TCP. It may be that due to the fast cooling rate (5°C/m), α-TCP phase could not revert back to the β phase.[28] Pierre[29] discussed the β-TCP→α-TCP transformation under different experimental conditions. It was found that[23] normally β→α-TCP transformation occurred at 1350°C and above. However, when β-TCP was heated up to 1348°C for 1 h and then quenched, it fully transformed to α-TCP. Interestingly, at a temperature of 1294°C, similar heating and cooling schedule resulted in a mixture of β-TCP and α-TCP. Comparable transformation took place with the starting phase as α-TCP. No transformation occurred at and below 1250°C starting with either α or β phase. However, Mackay[30] reported that β→α-TCP transformation upon heating occurred at 1180°C, which was lower than that reported by Pierre as well as in this investigation. In the present case, β→α-TCP transformation in the composites occurred at and above 1200°C. The FTIR results, presented in Fig. 5, also corroborate the XRD results. In case of HAp10M sample, the presence of O–H could be identified upto 1350°C, whereas for HAp30M samples the presence of O–H could not be identified even at 1200°C (Fig. 5(b)), indicating an almost complete decomposition of HAp to TCP at a lower temperature.

### *(2) Sintering Reactions*

In this subsection, the chemical reactions related to HAp dissociation and sintering in presence of mullite are discussed. Pure HAp starts to dissociate at about 900°C. However, HAp synthesized in an aqueous solution by the chemical route, was found to be more stable.[31] From the XRD data (Fig. 3(I)), it is revealed that pure HAp is quite stable upto 1200°C (Fig. 3(I)(c)). In presence of mullite, it starts dissociating at a much lower temperature as indicated by XRD data (Figs. 3(II–IV)). The possible reactions associated with the dissociation of pure HAp can be expressed as:

$$Ca_{10}(PO_4)_6(OH)_2 = 2\beta\text{-}Ca_3(PO_4)_2 + Ca_4P_2O_9 + \uparrow H_2O \quad (1)$$

$$Ca_{10}(PO_4)_6(OH)_2 = 3\beta\text{-}Ca_3(PO_4)_2 + CaO + \uparrow H_2O \quad (2)$$

Both the above reactions describe the formation of β-TCP, while the first reaction produces tetracalcium phosphate ($Ca_4P_2O_9$), the second one leads to the formation of CaO. The presence of CaO is confirmed from the XRD (Figs. 3II–IV), and also has been reconfirmed from the TEM diffraction pattern.[12] Therefore, in the present case, the later reaction is more likely. Additionally, the formation of the other calcium-alumino-silicate grain-boundary reaction products is the result of a limited reaction of CaO with mullite. The calcium-alumino-silicate liquid phase can crystallize into gehlenite ($C_2AS$) and alumina ($Al_2O_3$) at the grain boundary. The reaction can be written as:

$$4CaO + 3Al_2O_3 \cdot 2SiO_2 = 2(2CaO \cdot Al_2O_3 \cdot SiO_2) + Al_2O_3 \quad (3)$$

The feasibility of the above reaction will now be analyzed in the light of the equilibrium ternary phase diagram (projection in 2D) of CaO–$Al_2O_3$–$SiO_2$ system (Fig. 8), where different ternary phases are shown inside the triangle and the binary phases are indicated along the sides of the triangle. Different isothermal lines are indicated by the corresponding temperatures. It can be noted that the CaO–$Al_2O_3$–$SiO_2$ system is well investigated for various industrial and research application.[32] Lawrence[33] reported that the system CaO–$Al_2O_3$–$SiO_2$ formed a liquid phase at 1170°C with a proportion of $SiO_2$:$Al_2O_3$:CaO::62:14:24, in weight ratio. Similar type of information can be obtained from the ternary phase diagram[24] of the system. In Fig. 8, the eutectic temperature of 1170°C is marked by a circle of number 2 with $SiO_2$:$Al_2O_3$:CaO::62.2 :14.7:23.3, which matches closely with the composition in Lawrence.[33] Here, C, A, and S stand for CaO, $Al_2O_3$, and $SiO_2$ respectively. The amount of available CaO, a product of HAp dissociation, can be derived from Fig. 4(a). The relative amount of CaO and mullite can be marked on the tie line, connected between the CaO and mullite (A3S2) composition. For the HAp-10, -20, and -30 wt% compositions, the mullite and CaO positions are marked on

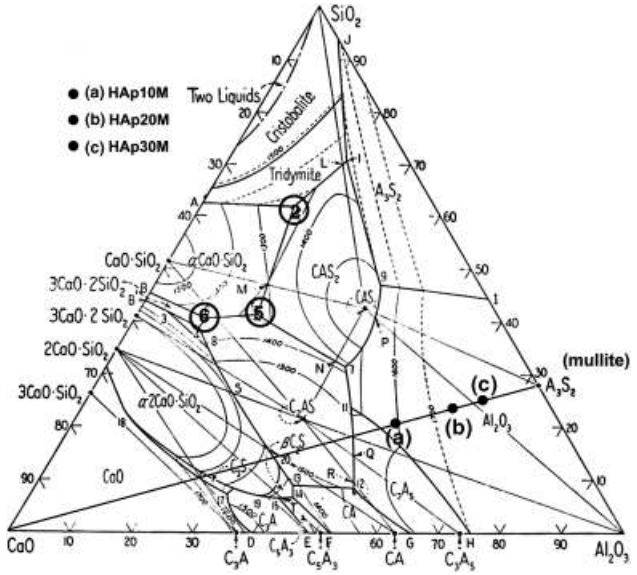


**Fig. 8.** Ternary phase diagram in the system CaO–$Al_2O_3$–CaO, showing various ternary phases present inside the triangle and binary phases along the sides. Isothermal lines are shown and marked by corresponding temperatures. The circles denoted by (2), (5), and (6) indicate three eutectic temperatures at and above which liquid phases of this system are present.[31] (a), (b), and (c) three points indicate the possible amount of mullite and CaO during sintering of hydroxyapatite (HAp)10M, HAp20M, and HAp30M composites, respectively.

the phase diagram (Fig. 8) as a, b, and c, respectively. The compositions were marked based on the amount of TCP (main peak) found in XRD results. If HAp dissociates to form TCP, the relative amount of CaO (dissociated product of HAp) can be calculated from the amount of TCP. The released CaO reacts with mullite. For the given amount of mullite, the relative amount of mullite and CaO can be marked in the ternary diagram, before they react. In Fig. 8 (phase diagram), the stable phases are gehlenite (C2AS) and alumina on the either sides of points a, b, and c. Therefore, it is possible that a part of mullite and CaO react and form gehlenite and alumina in the temperature range of 1170°–1350°C, as proposed in Eq. (3).

### *(3) Densification*

In this study, one of the main foci has been the effect of sintering temperature and composition on the densification behavior of the HAp/mullite composites. From the analysis of density and shrinkage (see Figs. 2(a) and (b).), it is clear that increasing the sintering temperature has at least three effects on the sintered density: (a) it increases the bulk density due to enhanced mass transport kinetics, (b) it reduces the theoretical density due to the transformation of HAp to TCP and c) it enhances the reaction between mullite and CaO (from the decomposition of HAp). Thus, the densification kinetics and the final sintered densities are the interplay among these three factors.

From the dilatometry results (Figs. 2(a) and (b)), it can be concluded that in HAp-mullite composites, both solid-state and liquid-phase sintering occurs at two different temperature intervals. Solid-stage sintering dominates at low temperatures (~800°–1150°C). There would be three types of interparticle contacts in the powder compact of composites.[25] These are HAp–HAp contacts, HAp-mullite contacts, and mullite–mullite contacts. As shown in Fig. 2, the densification behavior for pure HAp is characteristic of solid-state sintering and the densification stops around 1300°C, when the sample reaches near full density. For the HAp10M, similar to pure HAp, densification starts at 800°C (see Fig. 2). This is due to the contribution of HAp–HAp particle contacts. However, the total densification is limited. This is due to the constraint imposed on the densification of HAp due to the nondensifying mullite particles.[26,27,34,35] From Fig. 8, it is revealed that the lowest eutectic temperature in the $CaO–SiO_2–Al_2O_3$ system is 1170°C. However, at this temperature, the amount of liquid would be too small, and hence the shrinkage will not be significant. With an increasing temperature, the amount of liquid phase will increase and there is another eutectic point at 1310°C. Also from Fig. 8, it can be noticed that the low amount of CaO leads to the formation of liquid phase at 1310°C. For the HAp10M sample, as the amount of mullite is less and the mullite assisted dissociation of HAp is limited (see Fig. 8). All these aspects result in a small amount of CaO. Therefore, the extent of liquid-phase formation is negligible and HAp10M shows delayed densification as compared with HAp20M and HAp30M. For composites with higher amounts of mullite, comparing dilatometric data (Fig. 2), it is quite interesting that even after increasing the amount of the nondensifying phase (e.g., mullite), the shrinkage/densification behavior is not degraded due to the formation of the liquid phase. For example, liquid-phase sintering dominates in HAp20M with limited contribution from solid-state sintering of HAp. When the mullite content is further increased to 30 wt%, the behavior is very similar to that HAp20M with small difference. In the case of HAp30M composition, the amount of mullite is more than the optimal required and as a result, there are nondensifying mullite/mullite contacts leading to overall lower shrinkage than that for the 20 wt% composite. Similar results have been reported by Salamone *et al.*[36] The reduction in density at temperatures >1350°C is primarily due to the formation of α-TCP (11% volume expansion).

### *(4) Mechanical Properties*

In order to assess the properties of the newly developed composites with the earlier developed HAp-based materials, Table II provides a comparison of the basic mechanical properties. Comparing the toughness values, it is quite clear that the fracture toughness in mullite-containing composites is much improved than pure HAp and TCP. Also, the toughness reported for other HAp-based composites have been mostly evaluated by the indentation crack method, which overestimates the toughness values. The presence of mullite needles with a typical aspect ratio of 7–8, as revealed in Fig. 7, contribute to an increased toughness in the composite. Such a contribution should be similar to whisker-induced toughening i.e. crack deflection effect, as reported for $ZrB_2–SiC_w$ whisker-reinforced composites.[37] A comparison of the flexural strength values, presented in Table II reveals comparable or even better values for CaP-mullite

**Table II. Summary and Comparison of the Basic Mechanical Properties of Some Of the Earlier Investigated Calcium Phosphate (CaP)-Based Materials with the Newly Developed CaP-Mullite Composites**

| Materials | Processing conditions | Compressive strength (MPa) | Flexural strength (MPa) | Fracture toughness ($MPa \cdot m^{0.5}$) | References |
|---|---|---|---|---|---|
| Sintered HAp | 1300°C | 509 | 113 | — | Akao *et al.*[39] |
| | 1150°C, for 3 h | 308 | 61 | | |
| Sintered β-TCP | 1300°C | 648 | 137 | — | Akao *et al.*[40] |
| | 1150°C, for 3 h | 459 | 138 | | |
| Injection molded HAp | 1200°C, for 3 h | — | 60 | — | Cihlar and Tranec[41] |
| CaP (HAp/TCP) | 1100°C for 1 h | — | 48.7 | | Pattanayak *et al.*[42] |
| HAp | 1200°C for 1 h | — | 57.4 | — | Kothapalli *et al.*[43] |
| HAp | Gel casting, sintered at 1250°C | — | 84.6 | 0.95 (indentation) | Chen *et al.*[44] |
| HAp | Hot pressed, 1100°C | — | 87 | 0.95 (indentation) | Sung *et al.*[45] |
| HAp-$ZrO_2$ nanocomposites | for 1 h at 20 MPa | | 155 | 2.1 (indentation) | |
| HAp-$ZrO_2$ (20–60 wt%) | 1250°C, for 4 h | 51–115 | | | Volceanov *et al.*[46] |
| HAp-20 wt% $Al_2O_3$ | 1200°C, for 2 h, | — | 200 | 1.3 (indentation) | Kim *et al.*[47] |
| HAp-30 wt% $Al_2O_3$ | hot pressed in Ar | | | 1.7 (indentation) | Present work |
| Pure HAp | 1200°C for 2 h | 54 | | 0.6 (SEVNB) | Present work |
| CaP-mullite (20–30 wt%) | 1350°C for 2 h | 232–380 | 75–80 | 1.5 (SEVNB) 2.5 (indentation) | |

HAp, hydroxyapatite; TCP, tricalcium phosphate; SEVNB, single edge V-notched beam.

composites. Interestingly, a large variation in compressive strength data can be observed in Table II. Perhaps, the variation in sample dimensions and/or, processing route are the contributing factors. On comparing the literature results with the present work, it is quite clear that the compressive strength values for HAp20M and HAp30M composites are much improved (see Tables I and II). The improvement of the compressive strength values was due to the incorporation of mullite particles in the CaP matrix. From the above discussion, it should be clear that these newly developed composites possess a better combination of fracture toughness, flexural strength, and compressive strength. Therefore, in view of a good combination of the mechanical properties and the *in vivo* biocompatibility property,[38] it can be envisaged that the developed composites will provide a better solution over pure HAp/TCP/other CaP-based composites in clinical applications.

## V. Conclusions

This paper presents results on the sintering, densification mechanism, microstructure details, phase assemblages, and properties of newly developed CaP-mullite composites. Based on the experimental observations and analysis of the densification results, the following major conclusions can be drawn.

(a) HAp-mullite composites with $>90\%$ theoretical density can be obtained by pressureless sintering in the temperature range of 1300°–1350°C and without any sintering additives. Combining the results of XRD, TEM, and dilatometer, it has been confirmed that the densification of these newly developed composites occurs initially, by solid state sintering up to a temperature of 1150°C, followed by liquid-phase sintering at higher temperature. The presence of mullite needles and the residual microporosity is observed in the sintered microstructures.

(b) Based on the careful analysis of the shrinkage kinetics, it can be concluded that there is an optimal amount of mullite for liquid-phase sintering of the composites. The formation of sintering liquid (Ca–Al-silicate phase) has been described by the reactions between CaO, a dissociation produce from HAp phase, and mullite. This has also been consistent for different composite composition according to the equilibrium $CaO–Al_2O_3–SiO_2$ ternary phase diagram.

(c) Another important observation has been that the dissociation of HAp to TCP depends on both sintering temperature and mullite content. Higher mullite-containing composites are more prone towards dissociation to β and α-TCP.

(d) The combination of large compressive strength of close to 400 MPa and modest SEVNB fracture toughness of $\sim 1.5$ $MPa \cdot m^{0.5}$ indicate that the optimally sintered light-weight CaP-mullite composite material could be a useful bone replacement material.

## Acknowledgment

The part of this research work, reported in this manuscript, is carried out under the framework of Indo–US Joint Public-Private Networked Joint Center on Biomaterials for Health Care (Grant No. IUSSTF/JC/Biomaterials/15-2008/2008-09), funded by the Indo–US Science and Technology Forum. R. K. B. also acknowledges the travel support to visit IIT Kanpur provided by the forum.

## References

[1]B. D. Ratner, A. S. Hoffman, F. J. Schoen, and J. E. Lemons, *Biomaterials Science: An Introduction to Materials in Medicine*. Elsevier Academic Press, London, 2004.

[2]S. Nath and B. Basu, "Designing Biomaterials for Hard Tissue Replacement," *J. Korean Ceram. Soc.*, **45** [1] 1–29 (2008).

[3]S. Gautier, E. Champion, and D. B. Assollant, "Processing, Microstructure and Toughness of $Al_2O_3$ Platelet-Reinforced Hydroxyapatite," *J. Eur. Ceram. Soc.*, **17**, 1361–9 (1997).

[4]J. Li, B. B. Fartash, and L. Hermansson, "Hydroxyapatite—Alumina Composites and Bone-Bonding," *Biomaterials*, **16**, 417–22 (1995).

[5]R. R. Rao and T. S. Kannan, "Synthesis and Sintering of Hydroxyapatite–Zirconia Composites," *Mater. Sci. Engg. C*, **20**, 187–93 (2002).

[6]V. V. Silva and F. S. Lameiras, "Domínguez RZ. Microstructural and Mechanical Study of Zirconia-Hydroxyapatite (ZH) Composite Ceramics for Biomedical Applications," *Compos. Sci. Technol.*, **61**, 301–10 (2001).

[7]G. Goller, H. Demirkıran, and F. N. Oktar, "Demirkesen E. Processing and Characterization of Bioglass Reinforced Hydroxyapatite Composites," *Ceram. Int.*, **29**, 721–4 (2003).

[8]W. Suchanek, M. Yashima, M. Kakihana, and M. Yoshimura, "Hydroxyapatite/Hydroxyapatite-Whisker Composites Without Sintering Additives: Mechanical Properties and Microstructural Evolution," *J. Am. Ceram. Soc.*, **80** [11] 2805–13 (1997).

[9]I. Manjubala and M. Sivakumar, "In-Situ Synthesis of Biphasic Calcium Phosphate Ceramics Using Microwave Irradiation," *Mater. Chem. Phys.*, **71**, 272–8 (2001).

[10]M. I. Alam, I. Asahina, K. Ohmamiuda, K. Takahashi, S. Yokota, and S. Enomoto, "Evaluation of Ceramics Composed of Different Hydroxyapatite to Tricalcium Phosphate Ratios as Carriers for rhBMP-2," *Biomaterials*, **22**, 1643–51 (2001).

[11]D. C. Tancred, B. A. O. McCormack, and A. J. Carr, "A synthetic Bone Implant Macroscopically Identical to Cancellous Bone," *Biomaterials*, **19**, 1735–43 (1998).

[12]S. Nath, K. Biswas, and B. Basu, "Phase Stability and Microstructure Development in Hydroxyapatite–Mullite System," *Scr. Mater.*, **58** [12] 1054–7 (2008).

[13]W. Rathje, "Zur Kentnis de Phosphate: I. Uber Hydroxyapatite," *Bodenk Pflernah*, **12**, 121–8 (1939).

[14]S. R. Choi and N. P. Bansal, "Mechanical Behavior of Zirconia/Alumina Composites," *Ceram. Int.*, **31**, 39–46 (2005).

[15]M. Mizuno and H. Okuda, "VAMAS Round Robin on Fracture Toughness of Silicon Nitride," *J. Am. Ceram. Soc.*, **78**, 1795–801 (1995).

[16]K. Nakamoto, *Infrared and Raman Spectra of Inorganic and Coordination Compounds*, 4th edition, John Wiley & Sons, New York, 1986, 140pp.

[17]Y. Yang, K. H. Kim, C. M. Agrawal, and J. L. Ong, "Influence of Post-Deposition Heating Time and the Presence of Water Vapor on Sputter-Coated Calcium Phosphate Crystallinity," *J. Dent. Res.*, **82** [10] 833–7 (2003).

[18]Y. Yanga, K. H. Kima, C. M. Agrawal, and J. L. Onga, "Interaction of Hydroxyapatite–Titanium at Elevated Temperature in Vacuum Environment," *Biomaterials*, **25**, 2927–32 (2004).

[19]L. B. Kong, T. S. Zhang, J. Ma, and F. Boey, "Anisotropic Grain Growth of Mullite in High-Energy Ball Milled Powders Doped with Transition Metal Oxides," *J. Eur. Ceram. Soc.*, **23**, 2247–56 (2003).

[20]T. Huang, M. N. Rahaman, T. I. Mah, and T. A. Parthasarathay, "Anisotropic Grain Growth and Microstructural Evolution of Dense Mullite above 1550°C," *J. Am. Ceram. Soc.*, **83**, 204–10 (2000).

[21]S. Rochazka, J. S. Wallace, and N. Claussen, "Microstructure of Sintered Mullite–Zirconia Composites," *Commun. Am. Ceram. Soc.*, **66** [8] C125–7 (1983).

[22]K. Okada and N. Otuska, "Synthesis of Mullite Whiskers and their Application in Composites," *J. Am. Ceram. Soc.*, **74**, 2414–8 (1991).

[23]S. H. Hong and G. L. Messing, "Development of Textured Mullite by Templated Grain Growth," *J. Am. Ceram. Soc.*, **82**, 867–72 (1999).

[24]E. M. Levin, H. F. McMurdie, and F. P. Hallin *Phase Diagram for Ceramics. Fig 313*, Edited by K. Reser Margie, and H. Insley. The American Ceramic Society, Columbus, OH, 1956.

[25]A. Jagota, E. D. Boyes, and R. K. Bordia, "Sintering of Glass Powder Packings with Metal Inclusions," *Proc. Mater. Res. Soc. Symp.*, **249**, 475–80 (1992).

[26]O. Sudre, G. Bao, B. Fan, F. F. Lange, and A. G. Evans, "Effect of Inclusions on Densification: II, Numerical Model," *J. Am. Ceram. Soc.*, **75** [3] 525–31 (1992).

[27]O. Sudre and F. F. Lange, "The Effect of Inclusions on Densifcation: III, The Desintering Phenomenon," *J. Am. Ceram. Soc.*, **75** [12] 3241–52 (1992).

[28]X. Yin, M. J. Stott, and A. Rubio, "α- and β-Tricalcium Phosphate: A Density Functional Study," *Phys. Rev. B*, **68**, 205205, 8pp (2003).

[29]P. D. S. S. Pierre, "Constitution of Bone China: I, High Temperature Phase Equilibrium Studies in the System Tricalcium Phosphate–Alumina-Silica," *J. Am. Ceram. Soc.*, **36** [6] 243–58 (1954).

[30]A. L. Mackay, "A Preliminary Examination of the Structure of $\alpha$-$Ca_3(PO_4)_2$," *Acta Cryst.*, **6**, 743–44 (1953).

[31]J. Arends, J. Christoffersen, M. R. Christoffersen, H. Eckert, B. O. Fowler, J. C. Heughebaert, G. H. Nancollas, J. P. Yesinowski, and S. J. Zawacki, "Hydroxyapatite Precipitated from an Aqueous Solution: An International Multimethod Analysis," *J. Cryst. Growth*, **84**, 515–32 (1987).

[32]G. Gruener, D. D. Sousa Meneses, P. Odier, and J. P. Loup, "Influence of the Network on Conductivity in Ternary $CaO–Al_2O_3–SiO_2$ Glasses and Melts," *J. Non-Cryst. Solid*, **281** [1–3] 117–24 (2001).

[33]W. G. Lawrence, *Ceramic Science for the Potters*. Chilton Book Company, PA, USA, 223pp.

[34]R. K. Bordia and R. Raj, "The Sintering of $TiO_2$ ($Al_2O_3$) Composites: A Model Experimental Investigation," *J. Am. Ceram. Soc.*, **71** [4] 302–10 (1988).

[35]S. M. Salamone and R. K. Bordia, "Effect of Non-Densifying Inclusions on the Densification of Ceramic Matrix Composites"; p. 497 in *Sintering Technology*, Edited by R. M. German, G. L. Messing, and R. G. Cornwall, CRC press, Boca Raton, FL, USA, 1996.

[36]S. M. Salamone, L. C. Stearns, R. K. Bordia, and M. P. Harmer, "Effect of Rigid Inclusions on the Densification and Constitutive Parameters of Liquid Phase Sintered $YBa_2Cu_3O_{6+x}$ Powder Compacts," *J. Am. Ceram. Soc.*, **86** [6] 883–92 (2003).

[37]X. Zhang, L. Xu, S. Du, J. Han, P. Hu, and W. Han, "Fabrication and Mechanical Properties of $ZrB_2$–SiCw Ceramic Matrix Composite," *Mater. Lett.*, **62** [6–7] 1058–60 (2008).

[38]S. Nath, B. Basu, M. Mohanty, and P. V. Mohanan, "In Vivo Response of Novel Hydrxyapaitite-Mulite Composite: Results Upto 12 Weeks of Implantation," *J. Biomed. Mater. Res.: Part B*, **90B**, 547–57 (2009).

[39]M. Akao, H. Aoki, and K. Kato, "Mechanical Properties of Sintered Hydroxyapatite for Prosthetic Applications," *J. Mater. Sci.*, **16**, 809–12 (1981).

[40]M. Akao, H. Aoki, K. Kato, and A. Sato, "Dense Polycrystalline β-Tricalcium Phosphate for Prosthetic Applications," *J. Mater. Sci.*, **17**, 343–6 (1982).
[41]J. Cihlar and M. Tranec, "Injection Moulded Hydroxyapatite Ceramics," *Biomaterials*, **17**, 1905–11 (1996).
[42]D. K. Pattanayak, R. Dash, R. C. Prasad, B. T. Rao, and T. R. Rama Mohan, "Synthesis and Sintered Properties Evaluation of Calcium Phosphate Ceramics," *Mater. Sci. Engg. C*, **27**, 684–90 (2007).
[43]C. Kothapalli, M. Wei, A. Vasiliev, and M. T. Shaw, "Influence of Temperature and Concentration on the Sintering Behavior and Mechanical Properties of Hydroxyapatite," *Acta Mater.*, **52**, 5655–63 (2004).
[44]B. Chen, T. Zhang, J. Zhang, Q. Lin, and D. Jiang, "Microstructure and Mechanical Properties of Hydroxyapatite Obtained By Gel-Casting Process," *Ceram. Int.*, **34** [2] 359–64 (2008).
[45]Y. M. Sung, Y. K. Shin, and J. J. Ryu, "Preparation of Hydroxyapatite/Zirconia Bioceramic Nanocomposites for Orthopaedic and Dental Prosthesis Applications," *Nanotechnology*, **18**, 065602, 6pp (2007).
[46]A. Volceanov, E. Volceanov, and S. Stoleriu, "Hydroxiapatite—Zirconia Composites for Biomedical Applications," *J. Optoelec. Adv. Mater.*, **8**, 585–8 (2006).
[47]S. Kim, Y.-M. Kong, I.-S. Lee, and H.-E. Kim, "Effect of Calcinations of Starting Powder on Mechanical Properties of Hydroxyapatite–Alumina Bioceramic Composite," *J. Mater Sci.: Mater. Med.*, **13** [3] 307–10 (2002). □